analytical chemistry

Article

pubs.acs.org/ac

Plasmonic Nanopipette Biosensor

Jean-Francois Masson,*[,†,‡,§] Julien Breault-Turcot,[†,‡] Rita Faid,[†] Hugo-Pierre Poirier-Richard,[†] Hélène Yockell-Lelièvre,[†] Félix Lussier,[†] and Joachim P. Spatz[‡,∥]

[†]Department of Chemistry, Université de Montréal, C.P. 6128 Succ. Centre-Ville, Montreal, QC, Canada, H3C 3J7

[‡]Department of New Materials and Biosystems, Max Planck Institute for Intelligent Systems, Heisenbergstr. 3, 70569 Stuttgart, Germany

[§]Centre for Self-Assembled Chemical Structures (CSACS), McGill University, 801 Sherbrooke Street West, Montreal, QC, Canada, H3A 2K6

[∥]Department of Biophysical Chemistry, University of Heidelberg, Im Neuenheimer Feld 253, 69120 Heidelberg, Germany

Supporting Information

ABSTRACT: Integrating a SERS immunoassay on a plasmonic "patch clamp" nanopipette enabled nanobiosensing for the detection of IgG. A SERS response was obtained using a sandwich assay benefiting from plasmon coupling between a capture Au nanoparticle (AuNP) on a nanotip and a second AuNP modified with a Raman active reporter and an antibody selective for IgG. The impact of nanoparticle shape and surface coverage was investigated alongside the choice of Raman active reporter, deposition pH, and plasmonic coupling, in an attempt to fully understand the plasmonic properties of nanopipettes and to optimize the nanobiosensor for the detection of IgG. These probes will find applications in various fields due to their nanoscale size leading to the possibility of spatially and temporally addressing their location near cells to monitor secretion of biomolecules.

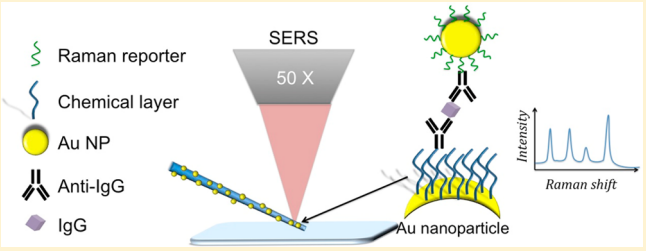

Intercepting chemical and biological messengers with spatial and temporal resolution is an important frontier of nanotechnology. The elucidation of the localization of biochemical molecules or ions within a cell, or monitoring chemical gradients between cells and the extracellular matrix, provides a wealth of information on cellular biology. Several tools are currently used to contribute to improving the knowledge on this important topic. Fluorescence microscopy has become an essential tool in biology, biochemistry, and medicine to study the localization of proteins in cells.[1] Additionally, fluorescence microscopy using quantum dots has been increasingly employed for imaging, labeling, and sensing various biomolecules within cells.[2] Furthermore, patch clamp techniques revolutionized the study of membrane receptors by providing real-time information about the function and role of these receptors in biological processes. Although these techniques are outstanding to study the biochemical processes within cells or the interactions of a cell with its environment, it remains difficult to apply these techniques for monitoring the secretion of proteins or metabolites other than electroactive neurotransmitters by the cell, or to monitor chemical gradients outside of cells with spatial and temporal resolution. Measuring chemical gradients outside cells is of outmost importance to investigate cell biology. Examples of applications include measuring the extracellular phosphorylation of proteins,[3] bacteria communication,[4] or ATP signaling.[5] This grand objective requires the development of novel nanoprobes capable of monitoring proteins or small molecules in the extracellular matrix, with high spatial and temporal resolution.

Nanobiosensing technologies are providing solutions to this challenge. Nanoelectrodes[6] and nanosensors based on electrochemistry are the most advanced technology for enzyme-based sensing, genosensors, and immunosensors.[7] Carbon fiber electrodes were developed in the 1990s to detect neurotransmitters within cells or secreted by cells.[8−10] Multimicroelectrode arrays were recently developed to address the challenge of multiplexing intracellular activity, recording from a single cell to a large numbers of cells.[11] Sensors based on biological nanopores provide information on molecular transport through a nanoscale opening.[12−14] This is especially adapted for nucleic acid analysis,[15] and the detection of a single DNA strand has been reported.[13] As nonscanning techniques, these biosensors provide valuable and local information on chemical processes.

Combining biosensing techniques with scanning probes in a single platform improves the applicability of sensors in applications requiring high spatial and temporal resolution. Scanning electrochemical microscopy (SECM) combines the sensing ability of nanoelectrodes with the spatial and temporal

Received: April 15, 2014
Accepted: August 19, 2014

   dx.doi.org/10.1021/ac501473c | *Anal. Chem.* XXXX, XXX, XXX−XXX

resolution of scanning probes to study biological processes occurring near cells. Using this technology, Bard and co-workers studied the respiratory cycle of *E. coli*.[16] SECM was also combined with atomic force microscopy (AFM) to benefit from the high spatial resolution of AFM microscopy using a nanoelectrode integrated on the tip of the cantilever to study ATP release from cells.[17] Recently, tip-enhanced Raman scattering (TERS) was proposed to achieve subdiffraction limit chemical imaging.[18] TERS probes served to assess the location of AuNP specifically bound to cell receptors, proving the capacity of TERS probes to work in close proximity to cells.[19]

Plasmonic nanosensors have matured toward versatile and sensitive techniques for the analysis of biomolecules.[20] For example, SERS immunoassays have been developed for numerous protein targets.[21,22] Plasmonic nanosensors have also been applied to a wide range of biophysical and bioanalytical studies,[23] and they have been adapted to detect molecules inside or around cells.[24] Wang et al. developed a plasmonic nanosensor array which was used to detect proteins secreted by cells.[25] The proteins were captured by arrays of Au nanodisks, and secondary detection with fluorescence revealed the location of regions of high IL-2 concentration. These techniques, however, are passively monitoring biomolecules near cells. The combination of the plasmonic sensing techniques on a SERS or TERS nanoprobe would enable nanobiosensing with higher spatial and temporal resolution.

One-dimensional nanoprobes based on cantilevers or pipettes were developed to investigate single cells[26] using electrochemical or optical techniques.[27] SERS nanoprobes are a promising tool to study cells and have been developed for intracellular studies using nanoparticle suspensions or with a SERS active nanopipette.[28] The SERS nanopipette was composed of a glass capillary decorated with AuNP to study the SERS spectra of the nucleus and cytoplasm.[29] In addition to this unique example, plasmonic nanopipettes are thus suited for multifunctional plasmonic sensing in various configurations. AuNP-coated nanopipettes can serve as a miniature plasmonic sensor, which could be stationed near cells to monitor extracellular content. The construction of plasmonic nanopipettes should not impair the use of standard electrochemical techniques employed near cells and using similar capillaries, such as SECM or scanning ion-conductance microscopy or patch clamp.

This article addresses the properties of plasmonic nanopipettes and demonstrates the potential for protein detection with this nanobiosensor, using IgG as a model biosensing scheme. However, this procedure could be generally applicable to all proteins with an existing ELISA assay, and this technological platform could be applicable to a variety of plasmonic biosensors based on SERS or metal-enhanced fluorescence. It could also be used in combination with other techniques performed on nanopipettes such as patch clamp and NSOM, providing a useful tool for the biophysical and biochemical study of cells.

EXPERIMENTAL DETAILS

We report here that a plasmonic nanosensor located on the tip of a nanopipette is suited for the detection of IgG (Scheme 1; See Supporting Information (SI) for complete description of the experiments). Glass capillaries, such as those used for patch clamp techniques, scanning near-field optical microscopy (SNOM), and TERS, were pulled to a tip diameter of approximately 500 nm using a pipet puller. The outer glass wall was modified with 3-aminopropyl triethoxysilane (APTES) to impart a positive charge on glass, and coated with Au nanoparticles (AuNP) to host an ELISA-like biosensor for proteins. Au nanospheres and Au nanoraspberries were synthesized respectively by citrate and HEPES reduction of Au salt (see SI for detailed procedure) and characterized using UV−vis spectroscopy and TEM. The Au NP suspensions were deposited at different pHs between pH 3 and 11, exploiting electrostatic interactions of the negative charge of the citrate or HEPES on the Au NP and the positive charge of the APTES-modified glass nanopipette. The nanopipettes were characterized with several techniques, including SEM to count Au NP surface coverage, SERS at 532, 633, and 785 nm with different Raman reporters (4-mercaptobenzoic acid, 4-mercaptophenol, rhodamine B, 5,5′-dithionitrobenzoic acid, and 11-mercapto-undecanoic acid), and dark-field microscopy.

Scheme 1. Concept of Nanobiosensing on the Tip of a Nanopipette[a]

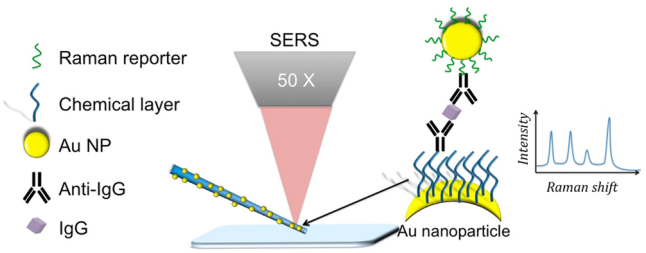

[a]AuNP hosting a capture antibody are immobilized on the nanopipette. Secondary protein detection is carried out with a AuNP modified with a Raman reporter molecule and a primary antibody selective for the analyte. The SERS signal of the Raman reporter is amplified by the plasmonic coupling between the pairs of AuNP and recorded with a Raman microscope.

The capture of IgG was monitored with a secondary detection step involving antibody and Raman reporter-modified AuNPs. IgG was captured on the plasmonic nanopipette by modifying the Au NP on the plasmonic nanopipette with 11-mercaptoundecanoic acid, followed by reactions with EDC-NHS, anti-IgG, ethanolamine, and BSA to create an IgG sensor. The secondary detection Au NPs were modified with 4-mercaptobenzoic acid for Raman detection, followed by functionalization with EDC-NHS, anti-IgG, ethanolamine, and BSA to yield an anti-IgG Au NP suspension. IgG solutions were prepared at 1 μM in PBS and reacted with the plasmonic nanopipette modified with anti-IgG, followed by secondary detection with the anti-IgG Au NP suspension. The assay readout was obtained using a confocal Raman microscope equipped with a 532, 633, or 785 nm laser, focused near the tip of the nanopipette with a 10× dry objective. SERS is typically performed in the longer wavelength range of the visible or in the near-infrared where intrinsic fluorescence or normal Raman scattering is minimal and biological molecules do not absorb. Although bulk equilibrium measurement are reported here on a timescale of a few tens of minutes, SERS can be measured in solution with time resolution of seconds, suited for real-time sensing near cells. For example, the copresence of the analyte and a Raman-active AuNP covered with the detection antibody can afford simultaneous capture and detection of the analyte. In addition, the localization of the nanopipette in close proximity of cells would significantly reduce mass transport time, the current limiting factor of the long assay time using SERS.

dx.doi.org/10.1021/ac501473c | *Anal. Chem.* XXXX, XXX, XXX−XXX

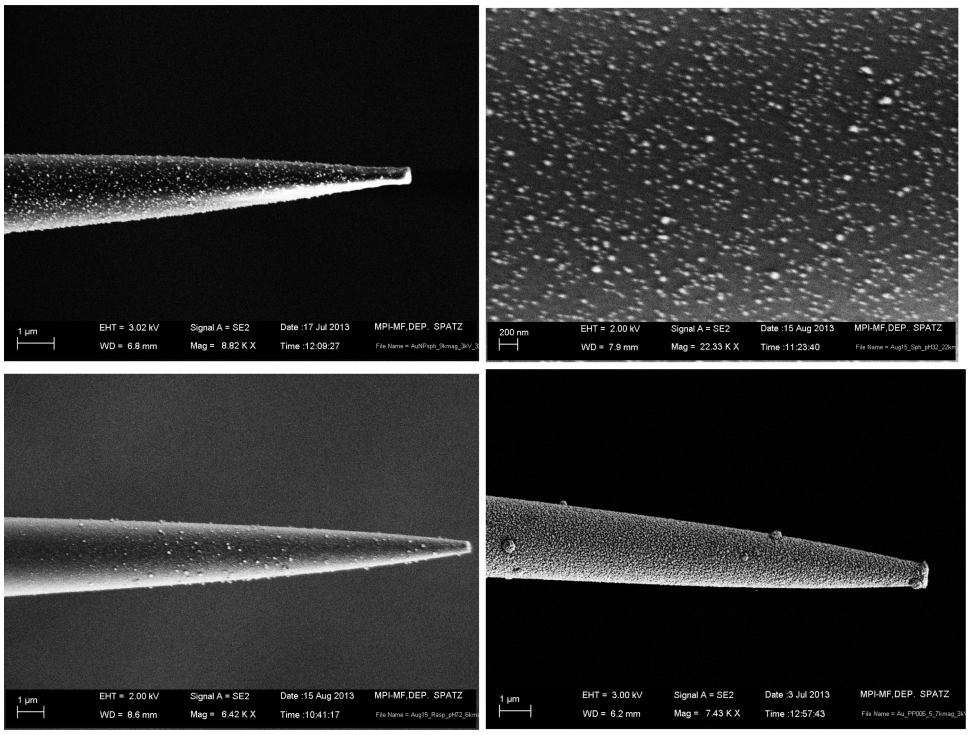

Figure 1. SEM images of the nanopipettes with Au nanospheres pH 3.2 (top left), a higher magnification SEM image of nanospheres pH 3.2 (top right), nanoraspberries pH 7.4 (bottom left), and Au film of 100 nm thickness (bottom right).

Table 1. SERS and Fluorescence Intensity of Raman Reporters Immobilized on the Plasmonic Nanopipette

	intensity for 532 nm[a] × 10^3 counts		intensity for 633 nm[b] × 10^3 counts		intensity for 785 nm[b] × 10^3 counts	
	sphere pH 3	rasp pH 7	sphere pH 3	rasp pH 7	sphere pH 3	rasp pH 7
DNBA	0.13 ± 0.02	7 ± 4	1.1 ± 0.1	0.36 ± 0.14	1.0 ± 0.6	1.4 ± 0.7
4-MBA	0.8 ± 0.5	1.9 ± 1.1	6.8 ± 1.7	0.21 ± 0.03	1.9 ± 0.7	0.25 ± 0.14
4-MP	0.9 ± 0.4	0.3 ± 0.2	4.3 ± 2.6	<LOD	1.3 ± 1.2	0.1 ± 0.07
RhB	36 ± 13	>65	4.3 ± 0.8	0.27 ± 0.1	1.1 ± 0.3	0.26 ± 0.12

[a]Fluorescence was observed for all Raman dyes at 532 nm. No Raman bands were distinguished except for spheres with 4-MBA and DNBA, but the intensity of these peaks was too weak to quantify. [b]Raman intensity measured for the most intense peak: DNBA: 1345 cm^{-1} ; 4-MBA: 1085 cm^{-1} ; 4-MP: 1085 cm^{-1} ; RhB:1653 cm^{-1} (1280 cm^{-1} for 785 nm)

RESULTS AND DISCUSSION

To achieve biosensing on the tip of nanopipettes, several factors must be considered. The nature of the plasmonic material deposited on the nanopipette, the selection of the Raman active reporter, and the laser excitation wavelength were evaluated for the plasmonic nanopipettes. Glass capillaries were pulled using a two-stage process on a P-2000 pipet puller (Sutter company) to reach a tip diameter of 484 ± 87 nm, diameter of the inside aperture of 308 ± 37 nm and a tip angle of 12.8° ± 0.8° (SI, Table SI1). The surface of the tip was modified with 3-aminopropyl triethoxysilane (APTES) to impart a positive charge to the surface of the nanopipette. Au nanospheres were synthesized via the citrate reduction of $HAuCl_4$[30], and Au nanoraspberries were obtained by reducing the gold salt with HEPES buffer adjusted to pH 7.4.[31] TEM analysis revealed that the nanospheres and nanoraspberries were 31 and 67 nm, respectively (SI, Figure SI1). Immersion of the APTES-modified nanopipette in a suspension of AuNP resulted in the electrostatic deposition of the AuNP onto the nanopipette. Nanospheres and nanoraspberries were deposited under conditions at pH 3.2 and 7.4, respectively. SEM images showed the presence of the AuNP on the glass surface of the nanopipettes (Figure 1).

The nature of the Raman active reporter will influence the sensitivity of the bioassays. In order to compare the plasmonic properties of varying plasmonic nanopipettes, different reporters were deposited on nanopipettes modified with nanospheres, nanoraspberries, and a thin Au film. Monolayers were formed with a series of mercaptobenzoic reporters (5,5′-dithionitrobenzoic acid (DNBA), 4-mercaptobenzoic acid (4-MBA), 4-mercaptophenol (4-MP)) and rhodamine B (RhB). Raman spectra were acquired with a laser excitation wavelength of 532, 633, and 785 nm. The SERS properties of the nanopipettes with AuNP were compared to a nanopipette modified with a 100 nm thick Au film. In all cases, the thin Au film yielded null responses (data not shown), whereas nanospheres and nanoraspberries were effective in generating a fluorescent or Raman signal.

When using a laser excitation wavelength of 532 nm, fluorescence dominated the spectral response for both nanospheres and nanoraspberries when using RhB as the Raman active molecule, despite the high probability of quenching due to the metal-fluorophore interaction (SI, Figure

dx.doi.org/10.1021/ac501473c | Anal. Chem. XXXX, XXX, XXX−XXX

SI4). The mercaptobenzoic reporters had a moderate fluorescent background for the nanoraspberries and low fluorescence was observed with the nanospheres at 532 nm. No Raman signal was observed for the reporters at this excitation wavelength, except for a weak signal for nanospheres coated with 4-MBA and DNBA. Therefore, due to the large fluorescent background obtained, 532 nm is not a suitable laser excitation wavelength for the SERS detection of nanopipettes.

When using a laser excitation wavelength of 633 and 785 nm, surface-enhanced Raman scattering dominated for the majority of Raman reporters and nanoparticle morphology combinations. The signal for nanospheres was more intense by about 1 order of magnitude than for nanoraspberries at 633 nm excitation wavelength and was roughly of the same magnitude for both nanoparticles at 785 nm (Table 1 − average intensity reported for n = 4 on individual nanopipettes). All reporters also led to SERS signals of the same order of magnitude, as the SERS intensity varied by about a factor of 5 from weakest to the strongest SERS for reporters analyzed in a set of condition (laser or AuNP shape). 4-MBA was the most intense reporter on nanospheres at 633 and 785 nm, followed by 4-MP, RhB, and DNBA. On nanoraspberries, DNBA led to the most intense SERS response at 633 and 785 nm excitation wavelengths followed by RhB, 4-MBA, and 4-MP (Table 1). 11-Mercaptoundecanoic acid (11-MUA), a common surface chemistry in biosensing, led to no SERS response at 633 nm but SERS was observed for 11-MUA at 532 nm excitation due to the absence of fluorescence at this excitation wavelength (SI, Figure SI5). Thus, 11-MUA would be appropriate for functionalizing the AuNP on the nanopipette as described below. Hence, SERS detection will be exclusive to the secondary detection step with a AuNP functionalized with a Raman active reporter. 4-MBA was selected for the functionalization of the secondary detection AuNP, due to the lowest fluorescence observed at 532 nm, the relatively high SERS intensity of the reporter at 633 and 785 nm, on both nanoraspberries and nanospheres, and the photostability of 4-MBA under laser excitation. It also provides a free carboxylic group to immobilize biomolecular receptors onto the nanoparticle using standard biochemical reactions commonly used in biosensing.

Understanding the plasmonic properties is important to exploit the nanopipettes as nanosensors. Suspensions of nanospheres and nanoraspberries exhibit a plasmon resonance at roughly 528 and 586 nm, respectively. However, the deposition method by electrostatic interactions can often lead to aggregation of the nanoparticles on the surface of the nanopipette. Dark-field spectroscopy revealed that the plasmon resonance is significantly red-shifted in comparison to the value in solution, resulting in a surface plasmon of 634 and 649 nm for nanospheres and nanoraspberries immobilized on the nanopipette. Thus, a significant fraction of AuNP aggregated on the nanopipettes, which will result in greater SERS intensity. In addition, dark-field experiments showed that the plasmon resonance of the nanospheres and nanoraspberries no longer differed significantly when deposited on the nanopipette. SEM images were acquired to estimate the number of AuNP immobilized on the nanopipettes (Figure 1). The nanopipettes were analyzed as prepared, with no further metal deposition. ImageJ was used to manually count the nanoparticles present in a square micrometer for at least four nanopipettes. A significantly larger number of nanospheres (~60−70 particles/μm^2) were deposited on the nanopipette than nanoraspberries (~10 particles/μm^2). Taking into account the relative size of nanoraspberries and nanospheres, and the area covered by AuNP exposed to the laser beam, we find that nanospheres cover about 0.046 μm^2 per square micron of surface, although nanoraspberries cover 0.035 μm^2 per square micron of surface. These values represent 4.6% and 3.5% of the surface of the nanopipette covered with, respectively, nanospheres and nanoraspberries, with nanospheres covering a greater area by about a factor 3/2. The SERS measurements should probe about 50% greater number of molecules on nanopipettes modified with nanospheres than nanoraspberries, as surface coverage of the Raman active reporter on the different AuNP should remain relatively equivalent (it has been reported that the surface coverage of thiolated ligands remains constant regardless of the size of NP[32,33]). However, the single-point measurement of the SERS response on nanopipettes modified with nanospheres and nanoraspberries differed by more than 50%. The SERS intensities of the Raman reporters were larger on nanospheres by almost an order of magnitude, which may be due to aggregation of nanospheres on the nanopipettes (see SEM images of Figure 1 and dark-field data).

The pH-dependent adsorption of AuNP with APTES-modified surfaces was studied to further understand the role of the surface-capping agent on the electrostatic adsorption process and to optimize the nanosensor. Electrostatic interactions of AuNP with the nanopipette depend on the deposition pH, which determines the charge on the APTES-modified nanopipette and of the capping agent on the AuNP. Similar studies have been reported with fluorescence-tagged NP bearing a permanent charge. Bouwstra et al. suggested that APTES-modified surfaces may have two pK_a values of 6.55 and 9.94.[34] In their work, the first pK_a led to a small loss of the negatively charged NP, whereas the second pK_a at 9.94 caused the largest decrease in NP adsorption. In opposition to fluorophore-tagged NPs reported elsewhere,[34] AuNP do not have a permanent charge at all pH values. Citric acid (pK_a of 3.1, 4.8 and 6.4) on the nanospheres is predominantly in the form of a citrate anion at a pH value larger than 3.1, while HEPES (pK_a of ~3 and 7.5) on the nanoraspberries is a zwitterion with an isoelectric point of roughly pH 5−5.5 (partial positive charge below, partial negative charge above the pI). Thus, the deposition pH of the AuNPs varied the nanoparticle coverage at the surface of the nanopipettes (Table 2). SEM images (SI, Figure SI2) revealed that a high coverage of citrate-capped nanospheres was observed at pH 3 (60−70 nanoparticles/um^2), although moderate AuNP coverage was noted from pH 5 to 9 (~20−50 nanoparticles/um^2) corresponding to the region of the first pK_a of the APTES-modified surface and partial loss of positive charge on the nanopipette. This resulted in a marked decrease of the AuNP coverage to less than 5 nanoparticles/um^2 at pH 11 due to the

Table 2. Plasmonic Properties of AuNP Deposited at Different pH Values on Nanopipettes

	λ_{SPR} (nm)		$\lambda_{dark\text{-}field}$ (nm)		coverage (particles/μm^2)	
pH	sphere	rasp	sphere	rasp	sphere	rasp
3	528	580	634	666	60−70	10−20
5	528	584	645	643	20−40	15−25
7	528	586	627	649	30−50	10
9	527	584	638	654	20−30	<5
11	527	548	606	640	<5	<5

dx.doi.org/10.1021/ac501473c | Anal. Chem. XXXX, XXX, XXX−XXX

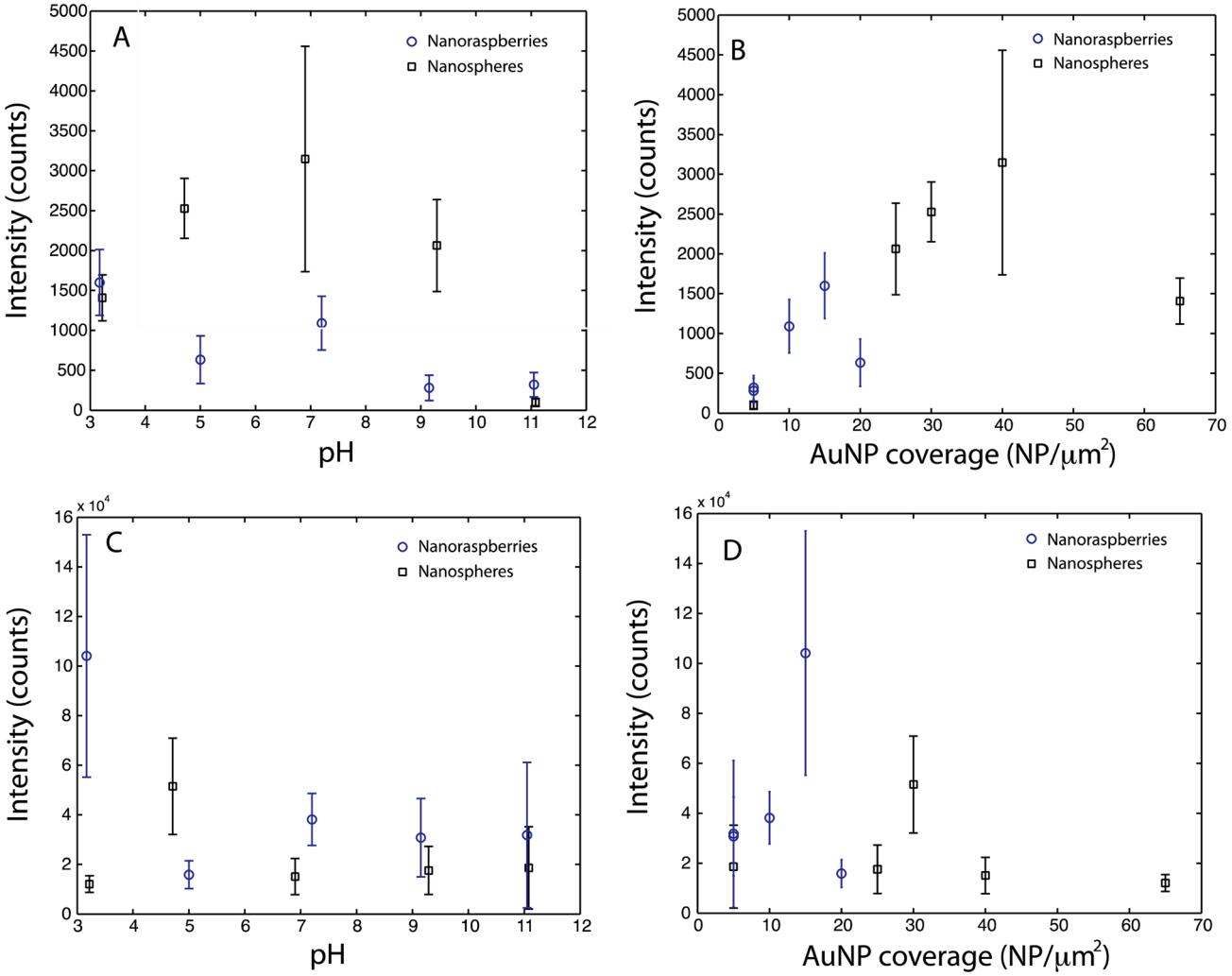

Figure 2. SERS intensity at 632.8 nm (A, B) and 785 nm (C, D) laser excitation wavelength for 4-MBA (1085 cm^{-1}) on nanospheres (black squares) or nanoraspberries (blue circles) deposited at various pH values on plasmonic nanopipettes. Panels A and C shown the influence of the deposition pH on the SERS intensity, and panels B and D correlate the AuNP coverage with the SERS intensity. It was observed that the SERS intensity increases with increasing AuNP coverage up to a maximal point (about 15 AuNP/μm^2 for nanoraspberries and about 30−40 AuNP/μm^2 for nanospheres). The SERS intensity represents the average value for four independent nanopipettes prepared in identical conditions and the error bars represent the standard deviation. Au NPs were deposited on the nanopipettes, followed by modification the Au surface with 4-MBA. Nanopipettes were not functionalized with biomolecules.

further loss of the positive charge on the nanopipette. Nanoraspberries had the highest AuNP coverage at a pH of 5 (15−25 nanoparticles/um^2), with a decreasing coverage for more acidic or basic pH values due to the increase of the positive charge on the AuNP at a more acidic pH and the decrease of the positive charge on the APTES-modified surfaces at a more basic pH. Nanoparticle coverage decreased to less than 5 nanoparticles/um^2 at pH values of 9 and 11. Thus, citrate-capped AuNP are more densely packed at lower pHs on the surface of the nanopipette, while due to the zwitterionic nature of HEPES, a pH of around 5 favors the deposition of AuNP. The presence of larger negative charge due to three carboxylate groups per citrate anion on the citrate-capped nanospheres may explain the higher coverage of nanospheres in comparison to nanoraspberries.

The plasmon resonance is a factor of size, shape, aggregation state, and refractive index of the surrounding media. The optical properties of AuNP were evaluated for the nanopipettes prepared at different deposition pHs. Suspensions of AuNP were prepared fresh before used, as stability of AuNP may vary at different pHs. UV−vis spectroscopy revealed that the resonance wavelength remained constant at 527−528 nm and thus nanospheres are stable for the short duration of the deposition process (Table 2, SI, Figure SI3). Suspensions of nanoraspberries at pH 3 did eventually aggregate after 1−2 days storage at 4 °C. Nanospheres were stable at pH 3−9 for the duration of the deposition process. In this case, the spectra of the nanoraspberries was relatively constant at 580 to 586 nm for pH 3−9, but the resonance wavelength decreased significantly at 548 nm for pH 11 (Table 2). The absorbance of the nanoraspberries deposited at pH 11 decreased significantly in addition to a blue-shift of the plasmon resonance (SI, Figure SI3). Dark-field spectroscopy revealed that the different deposition pHs did not significantly change the plasmon resonance on the surface of the nanopipette, except for nanospheres deposited at pH 11 (resonance wavelength at 606 nm). The plasmon resonance for nanospheres deposited between pH 3 and pH 9 varied from 627 to

dx.doi.org/10.1021/ac501473c | Anal. Chem. XXXX, XXX, XXX−XXX

638 nm, while nanoraspberries had resonances from 640 to 666 nm (Table 2). The scattering intensity was relatively constant for all deposition pH values. Aggregation explains the respective redshift of 100 and 60 nm for the plasmon resonances for nanospheres and nanoraspberries when in solution and on the nanopipette.

The SERS response depends on the several factors studied above, such as the AuNP coverage, aggregation state, and the wavelength of the plasmon resonance. Thus, the SERS response at 633 nm excitation wavelength for 4-MBA on the AuNP deposited on the nanopipettes depended on the pH at which the sensor was prepared (Figure 2A). The SERS intensity was optimal at pH 7 for nanospheres and at pH 3 for nanoraspberrries. *t* tests (n = 4 for each measurement, 95% confidence) for comparing means were performed to validate statistical difference between the SERS intensities at optimal pH with the SERS intensity at different deposition pHs. The *t* test discriminated the values for the optimal deposition pH of nanospheres with the SERS intensity obtained at low (pH = 3) and high pH (pH = 11) but was statistically equivalent for pH 5 and 9. For nanoraspberries, the *t* test revealed statistical difference of the SERS intensity with other deposition pHs of 5, 9, and 11. The plasmon resonance for both nanospheres and nanoraspberries deposited at different pHs matches quite well the 633 nm laser, which cannot explain the differences in SERS intensity for the deposition of AuNPs at different pHs. However, the SERS intensity was in good agreement with the particle coverage (Figure 2B). The SERS intensity increases with coverage for both nanospheres and nanoraspberries up to a AuNP coverage of about 10−20 NP/μm^2 for nanoraspberries and 30−50 NP/μm^2 for nanospheres. The linear increase of the SERS intensity at low particle coverage is in good agreement with the observation of Zhu et al.[35] The SERS intensity decreased to some extent at higher particle coverage than these maxima. We observe that this decrease in SERS intensity despite a higher surface coverage occurred near the pH of zero net charge for citrate (near pH 3) and for HEPES (near pH 5). The SERS intensity at 785 nm excitation wavelength was similar regardless of deposition pH and particle coverage. This absence of correlation of deposition pH or particle coverage with SERS intensity at 785 nm is likely due to the mismatch of the surface plasmon resonance with the laser wavelength. Thus, deposition pHs of 7 and 3 were selected for nanospheres and nanoraspberries, respectively, in the following experiments due to the highest SERS intensity obtained with 4-MBA.

Homogeneity of the SERS response at different locations was estimated with SERS images of 4-MBA on the nanopipettes with nanospheres and nanoraspberries deposited at pH 7 and 3, respectively. The SERS response was observed for the entirety of the tip of the nanopipette, with varying degree of intensity (Figure 3). The nanopipette with nanospheres showed a greater area of the nanopipette with high SERS intensity than for nanoraspberries. The higher coverage of nanospheres on the nanopipette may explain the greater homogeneity of the SERS signal. The beam diameter is approximately 1.1 μm with a 50X objective (NA = 0.7) and thus the area illuminated is nearly 0.96 μm^2. Thus, about 30−50 AuNPs are probed with nanospheres in comparison to 10−20 AuNP with nanoraspberries. Interrogating fewer AuNP may lead to greater inhomogeneity of the SERS response, as the number of AuNP in the beam spot is more likely to vary. The single-point measurements that were done previously included an alignment of the probe with scattering of the laser beam prior to the actual

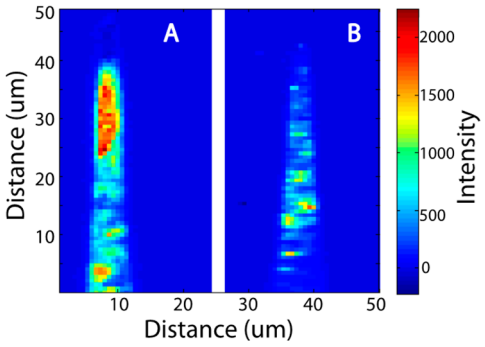

Figure 3. SERS imaging of nanopipettes with nanospheres deposited at pH 7 (A) and nanoraspberries deposited at pH 3 (B). The images were acquired for regions of 50 × 50 μm (25 × 50 μm is shown here), with pixel resolution of 0.67 μm using a 50× objective, 0.95 mW laser power at 632.8 nm, and 500 ms integration time per pixel.

measurement to optimize the position of the nanopipette. This confirmed that the nanopipette was colocalized between the beam path and high scattering region (higher SERS intensity). This reduces the variability of single point measurements. Despite the obvious advantages of the nanospheres, both types of AuNP were used for IgG detection to validate these conclusions with a relevant nanobiosensor.

Immobilizing anti-IgG on the AuNP of the nanopipettes created a plasmonic sensor. Standard reactions for SPR sensing of proteins were performed on the nanopipettes. 11-MUA was immobilized on the sensors due to the absence of SERS signal at 633 and 785 nm, followed by activation with *N*-ethyl-*N*′-(3-(dimethylamino)propyl) carbodiimide (EDC) and *N*-hydroxysuccinimide (NHS), and finally immobilization of anti-IgG and blocking with ethanolamine in a first step and BSA in a second step. 11-MUA is preferred to shorter linkers as SPR sensors demonstrated better sensitivity with longer alkyl chains thiols. Using shorter chain alkyl thiol would minimally change the distance of the AuNP dimer (less than 1 nm) in comparison to the large distance between the AuNP dimer resulting from the protein sandwich (15−20 nm). Depositing nanospheres, nanoraspberries, or a thin Au film created the different nanopipettes. The detection AuNP of the sandwich assay was synthesized by modifying AuNP with 4-MBA (Raman tag) and subsequently performing the same series of reactions as for the AuNP located on the nanopipette for the attachment of anti-IgG. The secondary detection AuNPs were nanospheres. The synthesis of nanoraspberries with anti-IgG was attempted but led to a high degree of aggregation. Thus, several sensors (n = 4) were constructed for each combination of nanopipettes with the Au film, nanospheres or nanoraspberries. The SERS response obtained for the detection of 1.1 μM IgG and a blank sensor (0 nM IgG) assessed the performance and selectivity of the sensor (Figure 4A). The blank sensors showed little nonspecific response from the secondary detection AuNP (Figure 4B shows weak 4-MBA response for the blank). IgG detection was carried out using a laser excitation wavelength of 633 and 785 nm with similar signal-to-noise. *t* tests for the comparison of two means (IgG detection and blank sensors) were used to assess the statistical validity of the detection with a 95% degree of confidence. Only the band at 1085 cm^{-1} was used for statistical comparison, as the Raman band associated with tryptophan and tyrosine of proteins (at 1605 cm^{-1}) interferes with the second Raman band of 4-MBA. Sensors using nanospheres as the secondary detection nanoparticle

dx.doi.org/10.1021/ac501473c | *Anal. Chem.* XXXX, XXX, XXX−XXX

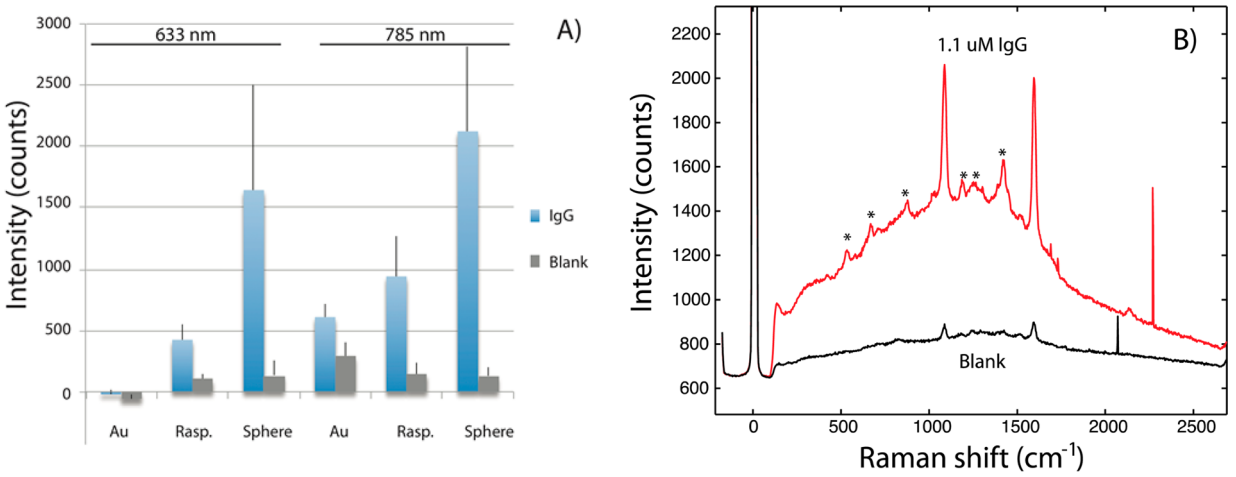

Figure 4. (A) SERS detection at 633 nm (left) and 785 nm (right) of IgG at 1.1 μM with plasmonic nanopipettes modified with nanospheres deposited at pH 7, nanoraspberries deposited at pH 3 or a thin Au film. The secondary detection in SERS was performed with nanospheres modified with anti-IgG and 4-MBA. Secondary detection with nanospheres led to a statistically significant measurement of IgG using nanopipettes with nanospheres and nanoraspberries. Other combinations did not afford IgG detection. The error bars represent the standard deviation of four nanopipettes prepared independently, each measured at a single location. (B) Typical SERS spectra for the detection of IgG (red curve) and a blank (black curve) nanobiosensor on the nanopipettes. The bands associated with proteins are denoted by *, and the strongest bands at 1085 and 1600 cm^{-1} are associated with 4-MBA. Note that there is a band for IgG at 1605 cm^{-1}, interfering with 4-MBA.

afforded statistically relevant detection. Nanopipettes with nanospheres led to a larger SERS intensity for IgG detection than nanopipettes with nanoraspberries. Au films on the nanopipettes led to weak SERS intensity, and no statistical difference was observed for the IgG and blank sensors. The weak SERS intensity for the IgG detection with the thin Au film may due to a poor hotspot excitation between a thin Au film and a AuNP on a nanopipette. Thus, the nanopipettes modified with AuNP afforded detection of IgG with the SERS immunoassay.

Several Raman bands associated with proteins were observed in the SERS spectra for the detection of IgG (Figure 4B). The Raman shifts reported for aromatic amino acids and for cysteine for anti-IgG on a roughened electrode[36] and for TERS on cells[19] are in good agreement with the Raman bands observed for the SERS spectra on the nanopipette (SI, Table SI2). Thus, proteins can be detected directly on the nanopipettes, similarly to the results of Vitol et al.[29] However, the construction of a biosensor for direct detection of proteins would need to rely on "non-protein" receptors (aptamers or moleculary imprinted polymers among others) to detect the Raman bands of proteins exclusively from the capture of the protein analyte and not from the antibodies usually employed in sandwich assays.

CONCLUSIONS

In conclusion, plasmonic sensing was performed on nanopipettes consisting of a pulled glass capillary similar to the ones used in patch clamp, SNOM, and TERS. IgG was detected near the tip of the nanopipette using a SERS sandwich assay with a detection AuNP labeled with a Raman active reporter. The electrostatic deposition process of AuNP was studied at various pH values for citrate-capped nanospheres and HEPES-capped nanoraspberries. It was revealed that a greater coverage of AuNP can be immobilized with citrate capped-nanospheres, but the surface coverage is relatively similar to nanoraspberries due to the larger size of the nanoraspberries. Dark-field spectroscopy demonstrated that the plasmonic resonances were similar for different deposition pH values, and that nanospheres and nanoraspberries were red-shifted from their solution resonances, indicating that aggregation occurred at the surface. Although the optimal deposition pHs depends on the charge of the AuNP and of the APTES-modified surface, the SERS response depends on the combination of aggregation state, plasmonic properties, and AuNP coverage. SERS was thus optimal near pH 7 for nanospheres and pH 3 was optimal for nanoraspberries. This sensing platform was demonstrated for protein detection but could be applied for several biosensing strategies using AuNPs with SERS or fluorescence detection. The nanoscale nature of the probe and the compatibility with microscopic techniques will facilitate measurements of biomolecules or metabolites near cells. We anticipate that multifunctional plasmonic nanosensors could also be integrated with SNOM, patch clamp, or TERS probes to further augment the local information obtained near cells. Therefore, these nanopipettes could find applications in biophysics, cell biology, chemical analysis, material science, and scanning probe techniques.

ASSOCIATED CONTENT

Supporting Information

Detailed experimental procedures, SEM images, and spectroscopic data are available as Supporting Information. This material is available free of charge via the Internet at http://pubs.acs.org.

AUTHOR INFORMATION

Corresponding Author

*E-mail: jf.masson@umontreal.ca. Tel.: +1-514-343-7342. Fax: +1-514-343-7586.

Notes

The authors declare no competing financial interest.

ACKNOWLEDGMENTS

The authors thank Witec, and D. Graham and K. Faulds (University of Strathclyde) for providing instrumentation time for some Raman measurements. The authors acknowledge

financial support from the Alexander von Humboldt foundation (Research fellowship for experienced researchers to J.-F.M.). J.-B.T. was supported by the Ministère de l'Enseignement Supérieur, de la Recherche et de la Science et de la Technologie (MESRST) of Quebec and the National Science and Engineering Research Council (NSERC) of Canada. J.P.S. is the Weston Visiting Professor at the Weizmann Institute of Science. This work is also part of the excellence cluster CellNetwork at the University of Heidelberg. Support from the Max Planck Society is greatly acknowledged.

REFERENCES

(1) Lippincott-Schwartz, J.; Snapp, E.; Kenworthy, A. *Nat. Rev. Mol. Cell Biol.* **2001**, *2* (6), 444−456.
(2) Medintz, I. L.; Uyeda, H. T.; Goldman, E. R.; Mattoussi, H. *Nat. Mater.* **2005**, *4* (6), 435−446.
(3) Yalak, G.; Vogel, V. *Sci. Signal.* **2012**, *5* (255), re7.
(4) Bassler, B. L. *Curr. Opin. Microbiol.* **1999**, *2* (6), 582−587.
(5) Schwiebert, E. M.; Zsembery, A. *Biochim. Biophys. Acta, Biomembr.* **2003**, *1615* (1−2), 7−32.
(6) Arrigan, D. W. M. *Analyst* **2004**, *129* (12), 1157−1165.
(7) Pumera, M.; Sánchez, S.; Ichinose, I.; Tang, J. *Sens. Actuators, B* **2007**, *123* (2), 1195−1205.
(8) Cahill, P. S.; Walker, Q. D.; Finnegan, J. M.; Mickelson, G. E.; Travis, E. R.; Wightman, R. M. *Anal. Chem.* **1996**, *68* (18), 3180−3186.
(9) Kawagoe, K. T.; Jankowski, J. A.; Wightman, R. M. *Anal. Chem.* **1991**, *63* (15), 1589−1594.
(10) Kennedy, R. T.; Huang, L.; Atkinson, M. A.; Dush, P. *Anal. Chem.* **1993**, *65* (14), 1882−1887.
(11) Spira, M. E.; Hai, A. *Nat. Nano* **2013**, *8* (2), 83−94.
(12) Zhang, B.; Zhang, Y. H.; White, H. S. *Anal. Chem.* **2004**, *76* (21), 6229−6238.
(13) Mara, A.; Siwy, Z.; Trautmann, C.; Wan, J.; Kamme, F. *Nano Lett.* **2004**, *4* (3), 497−501.
(14) Bayley, H.; Cremer, P. S. *Nature* **2001**, *413* (6852), 226−230.
(15) Venkatesan, B. M.; Bashir, R. *Nat. Nanotechnol.* **2011**, *6* (10), 615−624.
(16) Holt, K. B.; Bard, A. J. *Biochemistry (Mosc).* **2005**, *44* (39), 13214−13223.
(17) Kueng, A.; Kranz, C.; Lugstein, A.; Bertagnolli, E.; Mizaikoff, B. *Angew. Chem., Int. Ed.* **2003**, *42* (28), 3238−3240.
(18) Pettinger, B.; Ren, B.; Picardi, G.; Schuster, R.; Ertl, G. *Phys. Rev. Lett.* **2004**, *92* (9), 096101.
(19) Alexander, K. D.; Schultz, Z. D. *Anal. Chem.* **2012**, *84* (17), 7408−7414.
(20) Anker, J. N.; Hall, W. P.; Lyandres, O.; Shah, N. C.; Zhao, J.; Van Duyne, R. P. *Nat. Mater.* **2008**, *7* (6), 442−453.
(21) Han, X. X.; Zhao, B.; Ozaki, Y. *Anal. Bioanal. Chem.* **2009**, *394* (7), 1719−1727.
(22) Porter, M. D.; Lipert, R. J.; Siperko, L. M.; Wang, G.; Narayanana, R. *Chem. Soc. Rev.* **2008**, *37* (5), 1001−1011.
(23) Couture, M.; Zhao, S. S.; Masson, J.-F. *Phys. Chem. Chem. Phys.* **2013**, *15* (27), 11190−11216.
(24) Kumar, S.; Harrison, N.; Richards-Kortum, R.; Sokolov, K. *Nano Lett.* **2007**, *7* (5), 1338−1343.
(25) Wang, S.; Ota, S.; Guo, B.; Ryu, J.; Rhodes, C.; Xiong, Y.; Kalim, S.; Zeng, L.; Chen, Y.; Teitell, M. A.; Zhang, X. *Nano Lett.* **2011**, *11* (8), 3431−3434.
(26) Gao, Y.; Longenbach, T.; Vitol, E. A.; Orynbayeva, Z.; Friedman, G.; Gogotsi, Y. *Nanomedicine* **2013**, *9* (1), 153−168.
(27) Morris, C. A.; Friedman, A. K.; Baker, L. A. *Analyst* **2010**, *135* (9), 2190−2202.
(28) Vitol, E. A.; Orynbayeva, Z.; Friedman, G.; Gogotsi, Y. *J. Raman Spectrosc.* **2012**, *43* (7), 817−827.
(29) Vitol, E. A.; Orynbayeva, Z.; Bouchard, M. J.; Azizkhan-Clifford, J.; Friedman, G.; Gogotsi, Y. *ACS Nano* **2009**, *3* (11), 3529−3536.
(30) Brown, K. R.; Natan, M. J. *Langmuir* **1998**, *14* (4), 726−728.
(31) Xie, J.; Zhang, Q.; Lee, J. Y.; Wang, D. I. C. *ACS Nano* **2008**, *2* (12), 2473−2480.
(32) Elzey, S.; Tsai, D.-H.; Rabb, S. A.; Yu, L. L.; Winchester, M. R.; Hackley, V. A. *Anal. Bioanal. Chem.* **2012**, *403* (1), 145−149.
(33) Hinterwirth, H.; Kappel, S.; Waitz, T.; Prohaska, T.; Lindner, W.; Laemmerhofer, M. *ACS Nano* **2013**, *7* (2), 1129−1136.
(34) van der Maaden, K.; Sliedregt, K.; Kros, A.; Jiskoot, W.; Bouwstra, J. *Langmuir* **2012**, *28* (7), 3403−3411.
(35) Zhu, Z.; Zhu, T.; Liu, Z. *Nanotechnology* **2004**, *15* (3), 357.
(36) Grabbe, E. S.; Buck, R. P. *J. Electroanal. Chem. Interfacial Electrochem.* **1991**, *308* (1−2), 227−237.